Am J Physiol Heart Circ Physiol 292: H1245–H1253, 2007.
First published December 8, 2006; doi:10.1152/ajpheart.01069.2006.

CALL FOR PAPERS | *Oxygen Sensing: Life and Death of a Cell*

Laser microdissection and capture of pure cardiomyocytes and fibroblasts from infarcted heart regions: perceived hyperoxia induces p21 in peri-infarct myocytes

Donald E. Kuhn, Sashwati Roy, Jared Radtke, Savita Khanna, and Chandan K. Sen

Laboratory of Molecular Medicine, Department of Surgery, Davis Heart and Lung Research Institute, The Ohio State University Medical Center, Columbus, Ohio

Submitted 29 September 2006; accepted in final form 17 November 2006

Kuhn DE, Roy S, Radtke J, Khanna S, Sen CK. Laser microdissection and capture of pure cardiomyocytes and fibroblasts from infarcted heart regions: perceived hyperoxia induces p21 in peri-infarct myocytes. *Am J Physiol Heart Circ Physiol* 292: H1245–H1253, 2007. First published December 8, 2006; doi:10.1152/ajpheart.01069.2006.—Myocardial infarction caused by ischemia-reperfusion in the coronary vasculature is a focal event characterized by an infarct-core, bordering peri-infarct zone and remote noninfarct zone. Recently, we have reported the first technique, based on laser microdissection pressure catapulting (LMPC), enabling the dissection of infarction-induced biological responses in multicellular regions of the heart. Molecular mechanisms in play at the peri-infarct zone are central to myocardial healing. At the infarct site, myocytes are more sensitive to insult than robust fibroblasts. Understanding of cell-specific responses in the said zones is therefore critical. In this work, we describe the first technique to collect the myocardial tissue with a single-cell resolution. The infarcted myocardium was identified by using a truncated hematoxylin-eosin stain. Cell elements from the infarct, peri-infarct, and noninfarct zones were collected in a chaotropic RNA lysis solution with micron-level surgical precision. Isolated RNA was analyzed for quality by employing microfluidics technology and reverse transcribed to generate cDNA. Purity of the collected specimen was established by real-time PCR analyses of cell-specific genes. Previously, we have reported that the oxygen-sensitive induction of p21/Cip1/Waf1/Sdi1 in cardiac fibroblasts in the peri-infarct zone plays a vital role in myocardial remodeling. Using the novel LMPC technique developed herein, we confirmed that finding and report for the first time that the induction of p21 in the peri-infarct zone is not limited to fibroblasts but is also evident in myocytes. This work presents the first account of an analytical technique that applies the LMPC technology to study myocardial remodeling with a cell-type specific resolution.

laser microdissection and pressure catapulting; ischemia-reperfusion; left anterior descending artery; ventricular remodeling; laser capturing

SPATIALLY RESOLVED molecular analysis of infarcted myocardial tissue has been hindered by the lack of microdissection techniques to collect tissue samples with micron-level precision. To address this important limitation in analytical tissue biology, the laser capture microdissection (LCM) technology has been originated by the National Institutes of Health through collaboration between bioengineering and cancer pathology groups (4, 10). Under direct microscopic visualization, LCM permits rapid procurement of histologically defined tissue samples. The approach can be employed to collect pathologically defined (e.g., infarct core) tissue elements down to the resolution of a single cell. In general, in LCM, biological material is placed on a glass slide, or equivalent surface, and a thermoplastic membrane is placed in direct contact on top of the material. The laser beam source is positioned below the material, and the beam is focused through a microscope ocular lens onto the biological material on the slide. When the laser beam strikes the material, it is blasted off of the glass surface and melts onto the thermoplastic membrane. The thermoplastic membrane piece containing the blasted material is then physically isolated and the material collected (4, 10). Laser microdissection has opened a window to new technologies. A variant of LCM is laser microdissection and pressure catapulting (LMPC) (5). In LMPC, the biological material is placed directly on top of a thermoplastic polyethylene napthalate membrane that covers a glass slide or equivalent. The membrane acts as a support, or scaffolding, to allow for catapulting relatively large amounts of intact material at one time. A focused laser beam is used to cut out an area of the membrane and corresponding biological material, and the beam is then defocused and the energy used to catapult the membrane and material from the slide. A motorized robotic (RoboMover) stage is used to move the sample through the laser beam path to allow the user to control the size and shape of the area to be cut. The catapulted sample is generally captured in an aqueous media positioned directly above the cut area. The major advantages of LMPC over LCM are the increased amount of tissue captured in a given time, preserved cellular integrity, and the biological material obtained without direct user contact (3, 5). LMPC enables capture of biological material ranging from defined multicellular tissue elements to specific sections of cells and organs to cellular organelles (3, 5). For the most part, LCM has been applied for the study of cancer (2, 6, 7, 14, 21, 23). Recently, we have reported the first methodology study describing how LMPC can be employed to microdissect infarct and peri-infarct regions of the heart to spatially resolve biological events in the focally infarcted heart (20, 25).

Ischemia in the heart results in a hypoxic area containing a central focus of near-zero oxygen pressure bordered by tissue

Address for reprint requests and other correspondence: C. K. Sen, Davis Heart & Lung Research Inst., 473 W. 12th Ave., Columbus, OH 43210 (e-mail: chandan.sen@osumc.edu).

The costs of publication of this article were defrayed in part by the payment of page charges. The article must therefore be hereby marked "*advertisement*" in accordance with 18 U.S.C. Section 1734 solely to indicate this fact.

with diminished but nonzero oxygen pressures (30). These border zones extend for several millimeters from the hypoxic core, with the oxygen pressures progressively increasing from the focus to the normoxic region (28). Thus reperfusion with oxygen-rich blood results in highest ΔP_{O_2} at the core of infarction, resulting in reoxygenation injury. The ΔP_{O_2} at the peri-infarct region is not as high and induces perceived hyperoxia (24, 26, 27, 30). Induction of p21 (Waf1/Cip1/Sdi1) in cardiac fibroblasts of the peri-infarct region is a hallmark of perceived hyperoxia (30). Perceived hyperoxia triggers a myocardial remodeling response by inducing p21-dependent differentiation of cardiac fibroblasts to myofibroblasts (24, 26, 27). For focal events like myocardial infarction, it is important to dissect infarction-induced biological responses as a function of space. For example, it is important to precisely discriminate the events at the core of infarction from those that are at the periphery or peri-infarct region. Development of such understanding requires micron-level resolution of the surgical procedure for tissue collection. LMPC offers that capability. In this study, we sought to develop a novel LMPC-based technique to study gene expression in cardiomyocyte and cardiac fibroblast cell populations residing in specific regions of the infarcted heart. Furthermore, we asked whether perceived hyperoxia induces p21 in peri-infarct myocytes. This work presents the first account of an analytical technique that applies the LMPC technology to study ventricular remodeling after myocardial infarction with a cell type-specific resolution.

MATERIALS AND METHODS

Myocardial ischemia-reperfusion surgery. Male C57BL/6 mice were purchased from Harlan Technologies (Indianapolis, IN) and used at 10–12 wk of age. Experimental myocardial infarction was accomplished as described previously (20, 25, 27). The studies were approved by the Institutional Animal Care and Use Committee of the Ohio State University. Briefly, mice were anesthetized, placed on a 37°C heated small animal table, and ventilated with 100% oxygen-isoflurane at an appropriate rate and tidal volume. Cardiac electrophysiology was monitored by using a standard three-lead ECG setup, and changes in electrical conductance were measured by using PC PowerLab software (ADInstruments, Castle Hill). A left thoracotomy was performed via the fifth intercostal space to expose the heart. A 30-min occlusion of left anterior descending coronary artery was followed by reperfusion. Laser Doppler flow measurement was used to verify ischemia and reperfusion. Upon successful reperfusion, the thorax was closed and negative thoracic pressure was reestablished for survival. The mice were euthanized 2 or 7 days after reperfusion.

Cardiac tissue procurement and processing. The heart was cut laterally just above or below the infarcted area, and the tissue containing the infarcted area was frozen in optimum cutting temperature compound (OCT) using liquid N_2. The frozen mouse hearts were cut into 10-μm-thick sections using a Leica 3500S cryostat (Leica, Germany). The sections were placed on RNAZap-treated thermoplastic (polyethylene napthalate)-covered glass slides from PALM Technologies (Bernreid, Germany) and used immediately. One section was typically cut at a time and placed on the slide immediately before use to minimize RNA degradation.

Frozen sections were stained with one or more of the following stains as described in the respective figure legends: hematoxylin QS (Vector, Burlingame, CA) and eosin (OSU Stores, Columbus, OH). Hematoxylin-eosin (H&E) staining was done by placing 1–2 drops of hematoxylin QS on a section for 30 s, followed by a 1-s dip into eosin. Hematoxylin QS staining was carried out by adding 1–2 drops of hematoxylin QS to each section and incubating at room temperature for 30–60 s. Following either of these stains, the sections were rinsed in distilled water to remove excess stain and allowed to air dry for 3–5 min at room temperature.

Immunostaining for α-vimentin was done using a rapid, <10 min, staining protocol. Sections were incubated at room temperature for 3–5 min in a 1:2 dilution of the primary antibody (anti-α-vimentin, Sigma-Aldrich Chemicals, St. Louis, MO) in 2% goat serum. Primary antibody detection was accomplished by using the appropriate secondary antibody and RTU Vectastain Universal Quick kit (Vector). Following a brief rinse with phosphate-buffered saline, the sections were incubated for 3 min at room temperature with biotinylated pan-specific universal antibody. The sections were briefly rinsed again with phosphate-buffered saline and then incubated at room temperature for 2–3 min in the streptavidin-peroxidase complex reagent. The sections were again rinsed briefly in phosphate-buffered saline before incubating in peroxidase with nickel substrate solution until the desired intensity was reached. The sections were then rinsed briefly in distilled water and used immediately after drying for LMPC or mounted using VectaMount aqueous mounting solution. Microscopy was performed with the use of a Zeiss Axiovert 200M. The stained sections were photographed with a AxioCam MRc camera before performing LMPC.

LMPC. LMPC was performed using the laser microdissection system from PALM Technologies (Bernreid, Germany) containing a PALM MicroBeam and RoboStage for high-throughput sample collection and a PALM RoboMover [PALM RoboSoftware version 2.2 (20)]. Typical settings used for laser cutting were a beam size of 30 μm and laser strength of 30 mV. Myocyte and fibroblast tissues were cut and captured under a ×40 ocular lens using the RoboPC autocatapulting feature. Cut elements were catapulted directly into 25 μl of an RNA lysis solution (RNAqueous Micro kit; Ambion, San Antonio, TX) situated directly above the section.

RNA isolation and quality analysis. RNA from LMPC samples was isolated by using the RNAqueous Micro kit from Ambion according to the manufacturer's instructions. The lysis solution (25 μl) used to capture the catapulted tissue in LMPC was spun into a tube, and 75 μl

Table 1. *Primers, forward and reverse sequences, and amplicon size in base pairs*

Primers	Sequence	Size, bp
GAPDH		
Forward	ATG ACC ACA GTC CAT GCC ATC ACT	340
Reverse	TGT TGA AGT CGC AGG AGA CAA CCT	
Collagen Ia		
Forward	GTG TGA TGG GAT TCC CTG GAC CTA	140
Reverse	CCT GAG CTC CAG CTT CTC CAT CTT	
Collagen IIIa		
Forward	ACC CCC TGG TCC ACA AGG ATT A	170
Reverse	ACG TTC TCC AGG TGC ACC AGA AT	
α-Sarcomeric actin		
Forward	GTA CCC TGG TAT TGC CGA TCG TA	179
Reverse	GCC TCA TCA TAC TCT TGC TTG CTG	
α-Vimentin		
Forward	GAT TTC TCT GCC TCT GCC AAC CTT	139
Reverse	CAT TGA TCA CCT GTC CAT CTC TGG	
Cardiac MHC		
Forward	GAA CAT GGA GCA GAC CAT CAA GGA	247
Reverse	CCT TCA ACT GTA GCT TGT CCA CCA	
Cardiac troponin		
Forward	GAT CTC TGC AGA TGC CAT GAT GCA	150
Reverse	CAG TGC ATC GAT ATT CTT GCG CCA	
p21		
Forward	ACAGGAGCAAAGTGTGCCGTTGT	327
Reverse	GCTCAGACACCAGAGTGCAAGACA	

MHC, myosin heavy chain.

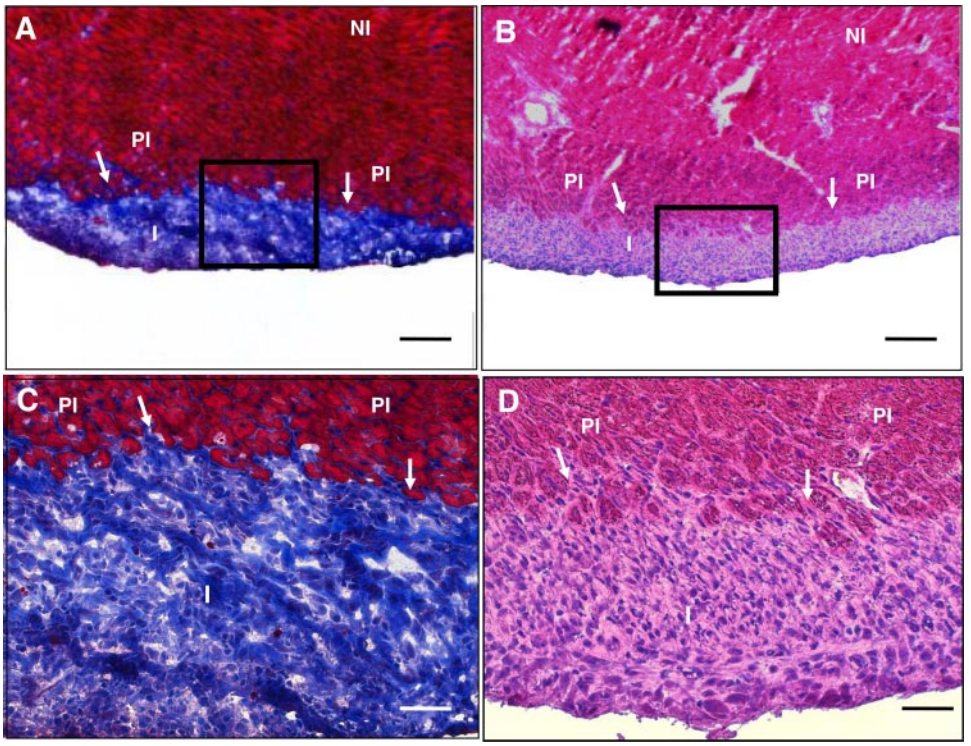

Fig. 1. Identification of infarct (I), peri-infarct (PI), and noninfarct (NI) regions in the ischemia-reperfused myocardium. Comparison of Masson-Trichrome (*A* and *C*) and truncated hematoxylin-eosin (tH&E; *B* and *D*) staining of serial sections from mouse hearts on *day 7* after ischemia-reperfusion. I, PI, and NI regions are marked. Although Masson-Trichrome staining results in brighter contrast of colors, tH&E is sufficient to visually identify I, PI, and NI. The rapidity of tH&E makes it a better-suited candidate for LMPC applications. *C* and *D*: enlarged area of the boxed areas shown in *A* and *B*. The arrows point to the boundary between infarcted and noninfarcted areas. Magnifications at ×50 (*A* and *B*), ×100 (*D*), and ×400 (*C*) are shown. Bars = 3.75 μm (*A*), 7.5 μm (*B* and *D*), and 30 μm (*C*).

of additional lysis solution were added. Three microliters of the supplied LCM additive were added to the lysis solution, followed by the addition of 129 μl of American chemical standard grade 100% ethanol. RNA was bound to silica-based spin-columns, and the columns were washed with the supplied buffers. RNA was eluted in 2 × 9 μl washes at room temperature for 5 min, each using either the supplied elution solution or nuclease-free distilled water preheated to 95°C. The RNA solution was then treated with DNAase for 20 min at 37°C. The quality and approximate quantity of the resulting RNA were determined by using the microfluidics system by Agilent Technologies (Agilent 2100 Bioanalyzer, Agilent Technologies) as described in the protocol provided for analysis using the "high-sensitivity" pico chip. In some cases, RNA quantity was measured by using the NanoDrop system (NanoDrop Technologies, Wilmington, DE) or the RiboGreen fluorescence dye assay (Molecular Probes, Eugene, OR).

Reverse transcription. RNA isolated as described in *RNA isolation and quality analysis* was reverse transcribed into cDNA using the Superscript III Reverse Transcription kit from Invitrogen (Carlsbad, CA). Eight out of twenty microliters of the RNA solution were used per reaction. Reactions were done using random hexamers. One microliter each of random hexamers (50 ng/μl) and dNTPs (10 mM) was added to 8 μl of RNA solution, and the resulting solution was incubated for 5 min at 65°C and then placed on ice for at least 1 min. Ten microliters of a 2× reaction mixture containing Tris·HCl (pH 7.4), 25 mM magnesium chloride, 0.1 M dithiothreitol, 40 units RNAse Out, and 200 units of Superscript III RT were then added. The resulting solution was incubated at 25°C for 10 min, followed by 50 min at 50°C, and finally at 85°C for 5 min. In some cases, RNA was degraded by further incubating for 20 min at 37°C with 2 units of RNAse H.

Quantitative real-time PCR of LMPC specimen. The cDNA synthesized in reverse transcription reactions was used directly for real-time PCR analyses (MX3000P system, Stratagene, La Jolla, CA). The gene-specific primers used in this study are listed in Table 1. The PCR

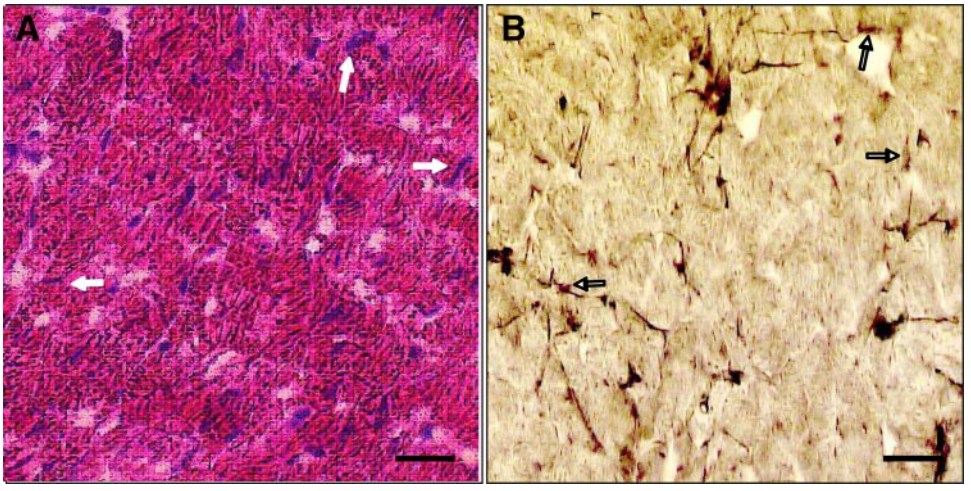

Fig. 2. Identification of fibroblasts using tH&E staining. Comparison of tH&E (*A*) and α-vimentin (*B*) staining of serial sections from postinfarcted mouse hearts on *day 2* after ischemia-reperfusion. The α-vimentin stain identified fibroblasts. The immunohistological approach employed to stain α-vimentin is not suited for laser microdissection pressure catapulting (LMPC) because of the length of time needed to stain. tH&E was sufficient to visualize myocytes and fibroblasts in the myocardium. The arrows point to cardiac fibroblasts. Magnification at ×400 is shown. Bars = 30 μm.

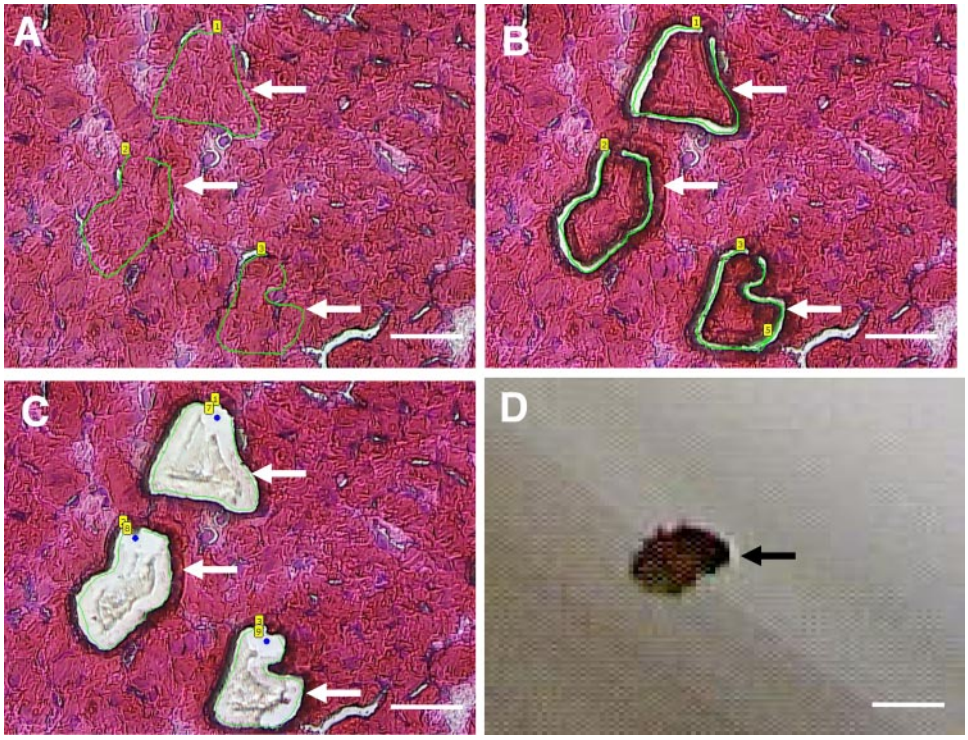

Fig. 3. Marking and catapulting of cardiomyocytes. In postinfarcted mouse hearts on *day 2* after ischemia-reperfusion, myocytes were identified by tH&E staining. *A*: the areas to be cut were marked with the specimen mounted on the laser microdissection system. *B*: result of the laser cutting with the elements separated from the section and ready to be catapulted. *C*: the tissue section after the cut elements have been catapulted. *D*: catapulted sections captured in a chaotrophic solution. Arrows in *A–C* point to identified areas containing only myocytes. The arrow in *D* points to one of the captured myocytes. Magnification at ×400 is shown. Bars = 30 μm.

reaction included 5 μl cDNA solution, 7.3 μl nuclease-free distilled water, 0.1 μl of each primer solution (50 μM), and 12.5 μl SYBR green real-time PCR mixture (Applied Biosystems, Warrington, UK). The solution was initially incubated at 50°C for 2 min, followed by 10 min incubation at 95°C to activate the polymerase. Typically, 40 cycles were then performed with steps of 45-s duration each at 95°C, 55°C, and 72°C. cDNA standards were used to determine relative quantities and to compare dissociation temperatures to partially ensure correct product formation. GAPDH gene expression was measured to correct for differences in extraction efficiency between samples.

Stability after sectioning and staining. Elements corresponding to a 1.0×10^6 μm^2 area were isolated from noninfarcted tissue for use in these experiments. The stability of GAPDH and α-sarcomeric actin genes was measured by incubating sections at room temperature, with

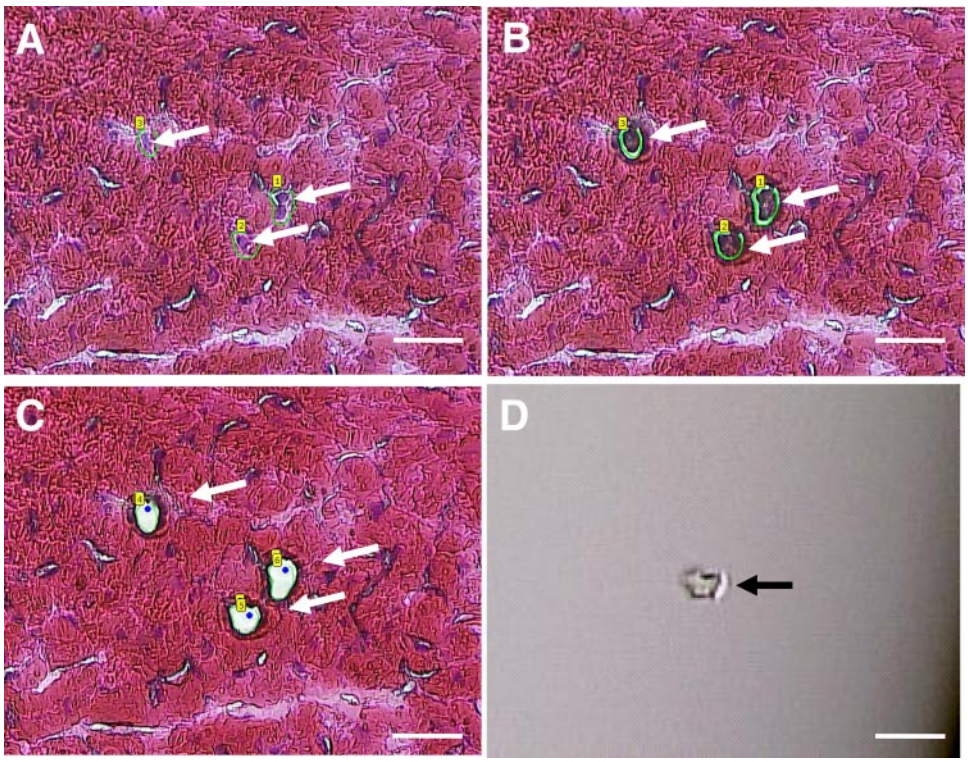

Fig. 4. Marking and catapulting of cardiac fibroblasts. In postinfarcted mouse hearts on *day 2* after ischemia-reperfusion, fibroblasts were identified by tH&E staining. *A*: the areas to be cut were marked with the specimen mounted on the laser microdissection system. *B*: result of the laser cutting with the elements separated from the section and ready to be catapulted. *C*: the tissue section after the cut elements have been catapulted. *D*: catapulted sections captured in a chaotrophic solution. Arrows in *A–C* point to identified areas containing only fibroblasts. The arrow in *D* points to one of the captured fibroblasts. Magnification at ×400 is shown. Bars = 30 μm.

no further manipulation, for specific time periods following staining. Four sections were placed on a polyethylene napthalate membrane-covered glass slide. Before the staining, one sample group was untreated and another was first dehydrated in a series of ethanol soaks followed by a 5-min xylene soak. Each slide was incubated dry for 0, 0.25, 1, or 3 h on the microscope stage.

Gene expression per area of myocyte tissue. Areas of sections corresponding to $10–100 \times 10^3$ μm^2 were cut from H&E-stained heart sections and captured in RNA lysis solution using LMPC as described in *Quantitative real-time PCR of LMPC specimen*. The RNA was isolated and used in reverse transcription reactions to prepare cDNA, and the cDNA was then used in quantitative RT-PCR to measure α-sarcomeric actin-specific gene expression as described in *Quantitative real-time PCR of LMPC specimen*.

Assessment of p21 gene expression. p21 Gene expression was measured in cardiomyocytes or cardiac fibroblasts isolated by LMPC from infarct, peri-infarct, and noninfarct areas of *day 2* ischemia-reperfused hearts as described in *Quantitative real-time PCR of LMPC specimen*. Approximately 1.5×10^5 μm^2 of cardiomyocytes and 0.6×10^5 μm^2 of cardiac fibroblasts were captured from each sample, and the RNA was isolated. Two 8-μl aliquots of the RNA were reverse transcribed into cDNA. The resulting solutions were combined, and nuclease-free distilled H_2O was added to give enough volume to perform 13 RT-PCR reactions from the cardiomyocyte samples and 8 from the cardiac fibroblast samples. The p21 primers, forward and reverse sequences, and amplicon size in base pairs are listed in Table 1.

Statistics. Values are expressed as means ± SD. The significance of difference between means was tested by using a two-tailed Student's *t*-test. The threshold of significance was set at $P < 0.05$.

RESULTS

We have developed a truncated H&E (tH&E) stain that rapidly and reliably detects the infarct- and peri-infarct regions of the ischemia-reperfused heart. This can be verified by Masson-Trichrome staining of serial sections (Fig. 1). Both stains identified the same infarct, peri-infarct (<300 μm area adjacent and parallel to the infarct border), and noninfarcted (>1,500 μm from the infarct border) areas. Primary considerations that need to be addressed while developing a staining procedure which is compatible with LMPC and subsequent genetic analyses are *1*) rapidity (preserving integrity of the cellular genetic material), *2*) an avoidance of harsh conditions that may disintegrate the cell and cause loss of cellular content, *3*) a reliable identification of infarct and noninfarct regions, and *4*) a distinguishing between cardiomyocytes and cardiac fibroblasts. The tH&E stain standardized in this work meets all of the above-said criteria by avoiding long incubation times and treatment with ethanol and xylene used during a standard H&E staining protocol. One of the primary goals of this study was to obtain relatively pure fractions of cardiomyocytes and cardiac fibroblasts possessing intact RNA, which would lend itself to real-time PCR analyses. Standard immunohistochemical approaches were not suitable (results not shown). The long incubation and several washing procedures were associated with marked degradation of RNA even if the staining was performed in the presence of RNAase inhibitors. To test whether the tH&E protocol reliably detects cardiomyocytes and cardiac fibroblasts, serial sections were stained with our tH&E stain and an anti-α-vimentin, the latter being a standard marker of cardiac fibroblasts. Immunohistochemical staining procedures are typically time consuming and do not lend themselves for LMPC applications (20). tH&E is a nonspecific stain but enables visualization of cardiomyocytes and cardiac fibroblasts (Fig. 2). We noted that the tH&E staining procedure enabled reliable visualization of cardiac fibroblasts (Fig. 2). Myocytes were readily identified by the tH&E stain as areas not containing cardiac fibroblasts (Fig. 3*A*). Cardiac fibroblasts were observed in the interstitial space between the myocytes. These results represent suggestive evidence supporting the hypothesis that the tH&E staining procedure was effective in reliably identifying the myocytes and fibroblasts. Additional experiments were therefore conducted to test the hypothesis more conclusively.

Cardiomyocytes from *day 2* ischemia-reperfused hearts were identified by using tH&E stain and were physically captured by using LMPC. Figure 3*B* shows the myocyte areas identified in the tissue section. The marked myocytes area were microdissected (Fig. 3, *B* and *C*) and captured (Fig. 3*D*). Visually, each element was clearly separated from the main section and did not contain any fibroblasts. The microdissected cardiomyocyte elements typically contained 400–800 μm^2 of myocytes. Once dissected, these elements were catapulted and captured in an RNA lysis solution (Fig. 3, *C* and *D*). A similar approach was

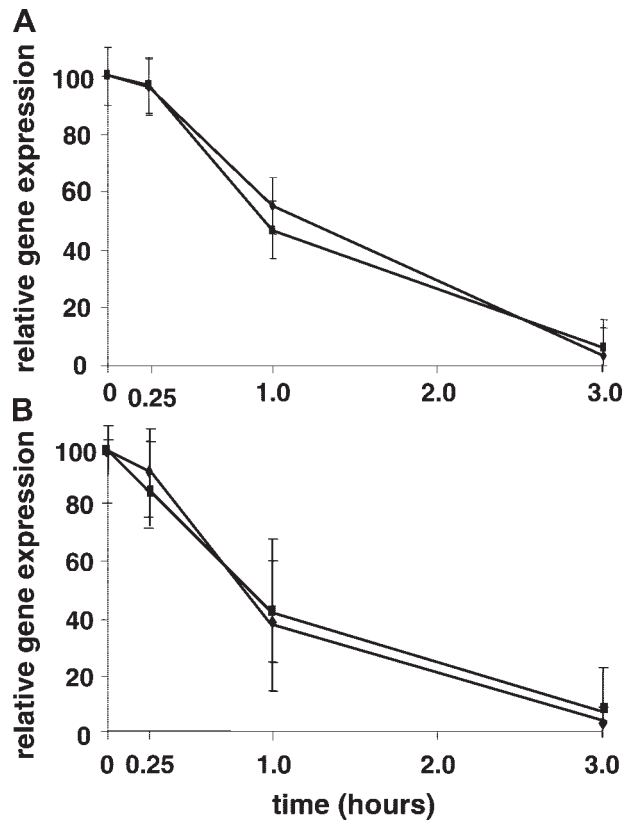

Fig. 5. Stability of RNA in tissue sections as a function of time following staining. Four sections were cut from postinfarcted mouse hearts on *day 7* after ischemia-reperfusion. *A*: sample untouched before staining. *B*: samples were first fixed in cold acetone followed by dehydration in a series of ethanol and xylene washes before staining. Noninfarcted regions corresponding to 2×10^6 μm^2 were identified by using the tH&E stain and then cut and captured immediately. RNA was extracted from the captured tissue and reverse transcribed into cDNA. The cDNA was used in real-time PCR using primers specific for GAPDH (♦) and α-sarcomeric actin (■). Both randomly selected genes were equally affected by time. Relative gene expression was calculated by setting the zero time value to 100 and then scaling the other time point values accordingly.

employed to collect pure cardiac fibroblasts from the myocardium. Myocyte contamination in fibroblast samples was avoided. Cardiac fibroblast elements (Fig. 4*D*) averaged 30–60 μm^2 in size. Fibroblasts were identified employing tH&E staining (Fig. 4*A*). To confirm the identity of the specific cell type being captured, the immediately succeeding serial section was stained for vimentin. The identified cells were microdissected cleanly, isolating fibroblasts from the myocardium (Fig. 4*B*). The excised elements were then catapulted and captured (Fig. 4, *C* and *D*). RNA stability in the tissue samples microdissected and captured represents a major concern, especially when the goal is to perform quantitative analyses of gene expression. We noted that the RNA quality in the tissue sections sharply deteriorated as a function of time (Fig. 5). Sections were allowed to air dry at room temperature and remain in that condition during the time course of the experiment. In addition, we tested whether an acetone fixation step, followed by a dehydration of the sections before staining, would lead to better RNA stability. The results were the same for both genes measured under either condition. This observation underscores the need for rapid staining procedures if LMPC followed by analysis of gene expression is the goal.

To determine the amount of myocytes necessary to execute analysis of gene expression, we isolated RNA from cumulative element sizes, ranging from 10×10^3 to 100×10^3 μm^2. Measurable gene expression was linear over this range (Fig. 6*A*). Our standard protocol provides enough RNA to perform 10 separate RT-PCR reactions, even when starting with 10×10^3 μm^2 element area. From 100×10^3 μm^2 element area, one can perform at least 100 RT-PCR reactions. Thus a considerable amount of gene expression data may be generated from such a small sample size. The amount of fibroblast sample needed for measuring gene expression using our protocol was determined by using α-vimentin gene expression, a well-known fibroblast marker. The expression of α-vimentin gene was linear over an area range of $30–100 \times 10^3$ μm^2. In excess of 30 separate RT-PCR reactions can be performed when starting with 100×10^3 μm^2 area of fibroblasts. An objective characterization of the purity of the cardiomyocyte and fibroblast cell population collected using our tH&E-LMPC technique was performed by assaying for genes specific for myocytes, fibroblasts, endothelial cells, and macrophages. Real-time PCR of laser-captured myocytes and fibroblasts was tested for the presence of CD68 (macrophage marker) and CD31 (endothelial cell marker). These genes were not detectable in both myocytes as well as fibroblast populations captured from the myocardium (data not shown). These results indicate that the laser-captured material was free of macrophages and endothelial cells. We selected three genes as myocyte-specific markers. They were cardiac myosin heavy

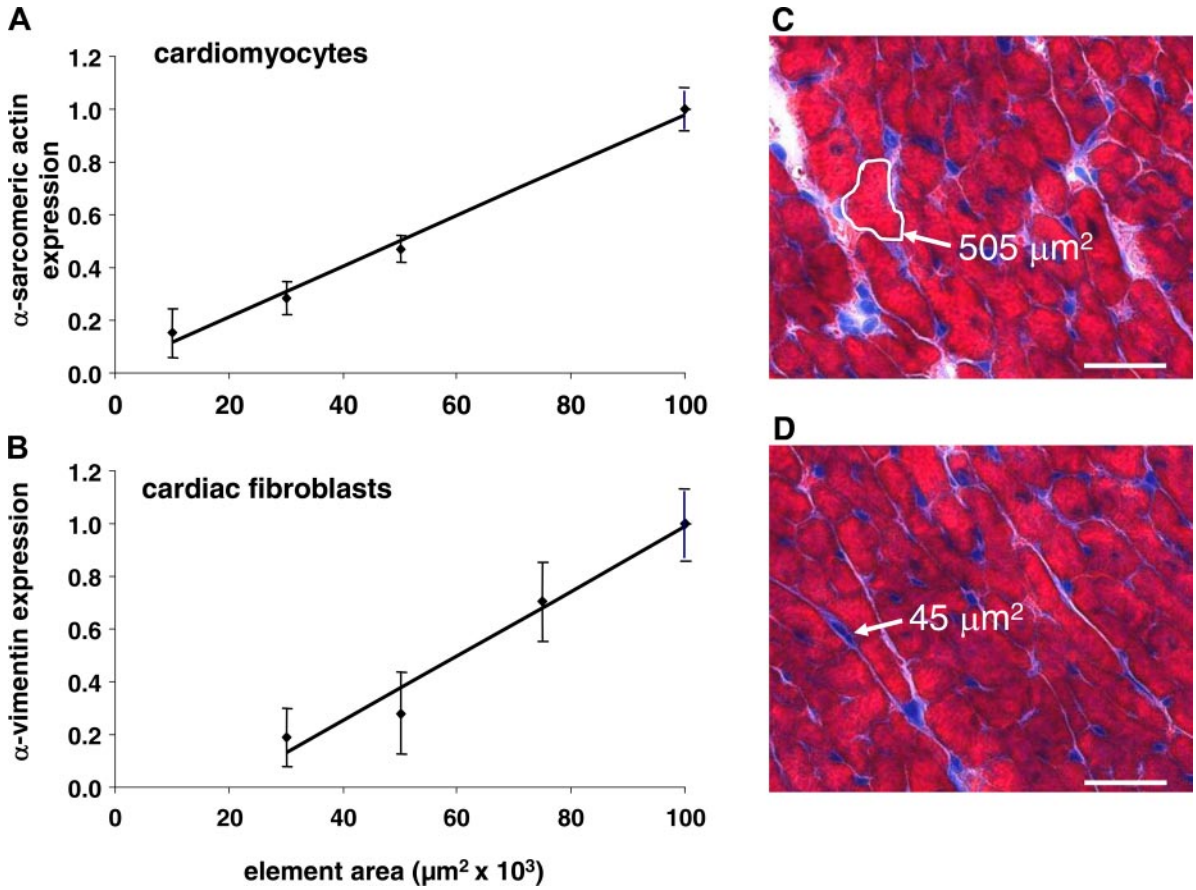

Fig. 6. Quantitation of gene expression in laser captured cardiomyocyte and cardiac fibroblast populations: threshold of captured element size required to perform real-time PCR. Myocytes and fibroblasts were captured from tH&E-stained myocardium sections. Element size ranging from 10×10^3 μm^2 to 100×10^3 μm^2 in area was cut and collected. *A*: relative gene expression of α-sarcomeric actin in cardiomyocytes. *B*: relative gene expression of α-vimentin in cardiac fibroblasts. Element size of a single myocyte (*C*) or fibroblast (*D*) is shown.

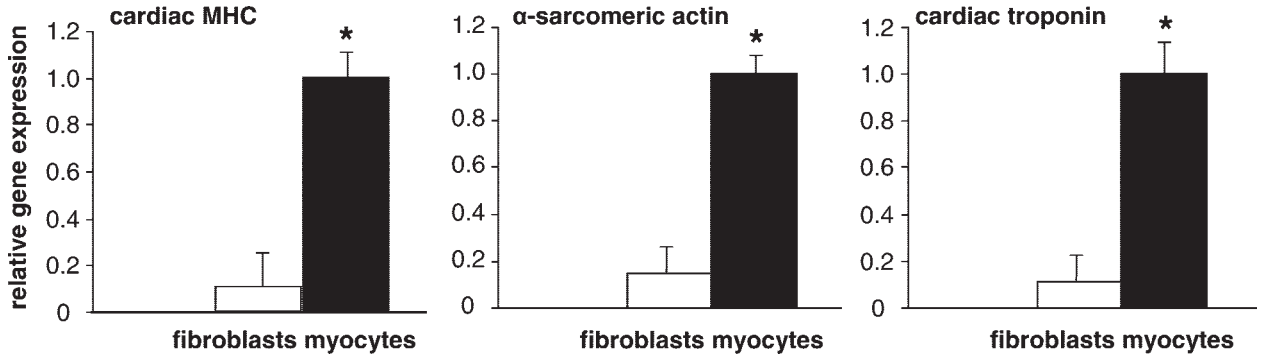

Fig. 7. Characterization of the purity myocytes and fibroblasts captured from the ischemia-reperfused heart: abundance of myocytes-specific genes in each of the 2 populations. *$P < 0.0001$, significantly different from corresponding value in the fibroblast population. MHC, myosin heavy chain.

chain, α-sarcomeric actin, and cardiac troponin I. Similarly, three genes with a high abundance in fibroblasts were examined as fibroblast markers. These genes were α-vimentin, collagen IA, and collagen IIIA. Myocytes laser captured from the myocardium were rich in myocyte-specific genes. The abundance of these genes in the laser-captured fibroblasts was low (Fig. 7). Captured fibroblasts showed high levels of fibroblast-specific markers. Myocytes showed very low abundance of these genes (Fig. 8). These observations indicate that the currently developed technique (Fig. 9) was effective in capturing pure populations of myocytes and fibroblasts from the myocardium.

Previously, we have reported that in the peri-infarct region of ischemia-reperfused heart, perceived hyperoxia induces the expression p21, which in turn leads to differentiation of the fibroblasts at that site to myofibroblasts (24–27, 30). Here, we sought to apply our LMPC technique to investigate whether p21 is also induced in myocytes located in the peri-infarct region. The noninfarct region, as defined in Fig. 1, was used as a control. Consistent with previously published data from mixed heart tissue and cultured fibroblasts (24–27), fibroblasts captured from the infarct region of the ischemia-reperfused heart had significant upregulation of p21 expression (Fig. 10). Induction of p21 expression in the peri-infarct region was also noted in myocytes (Fig. 10). This observation establishes that, following ischemia-reperfusion, p21 is induced in both fibroblasts as well as myocytes in the peri-infarct region.

DISCUSSION

Focal ischemia-reperfusion in the heart causes changes in the myocardium that varies depending on the distance of the site from the focal point or the infarct core. Regions of myocardial infarct are surrounded by a border peri-infarct zone that is perfused but challenged by the ischemia-reperfusion event. Although systolic dysfunction has been attributed to elevated wall stress in this region, there is evidence that intrinsic abnormalities of contractile performance exist in the peri-infarct region of the myocardium (16). In many ways, biological responses in the infarct core are different from those noted in the peri-infarct region (9, 17, 18). Ventricular arrhythmias have been shown to originate in the myocardial peri-infarct region due to irregular heterotopic conduction. Hypoperfused but viable myocardium is often localized in those areas and may be involved in the pathogenesis of arrhythmias (18). Energy insufficiency in the peri-infarct region may contribute to the transition from compensated left ventricular remodeling to congestive heart failure (16).

Unlike the infarct core, the peri-infarct tissue is challenged but viable (9). A specific study of the peri-infarct region is therefore crucial to understand the myocardial healing response (11, 17, 31). The peri-infarct region is a target for therapeutics aimed at myocardial healing (29, 32). In our previous works, we have hypothesized that whereas oxygen toxicity is a major contributor to injury in the ischemia-reperfused infarct core, sublethal oxygen insult in the peri-infarct region induces fibro-

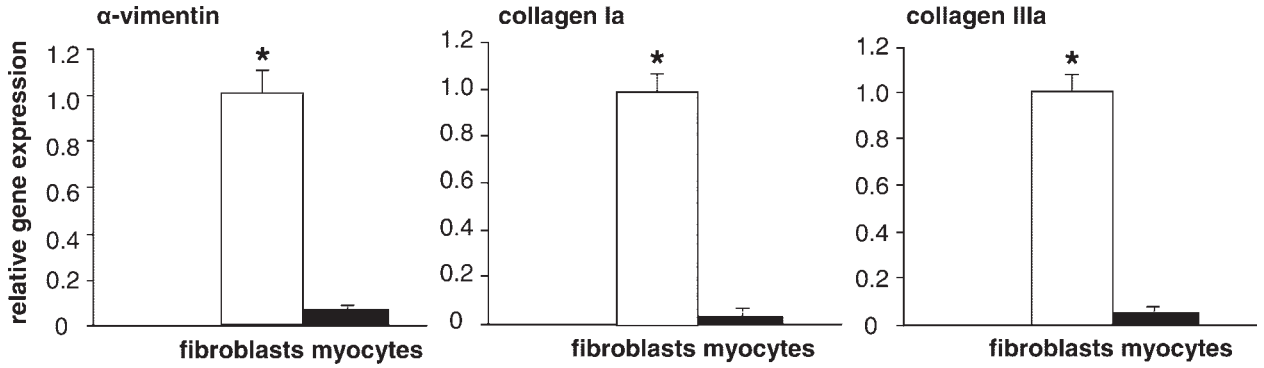

Fig. 8. Characterization of the purity myocytes and fibroblasts captured from the ischemia-reperfused heart: abundance of fibroblast-specific genes in each of the 2 populations. *$P < 0.0001$, significantly different from corresponding value in the fibroblast population.

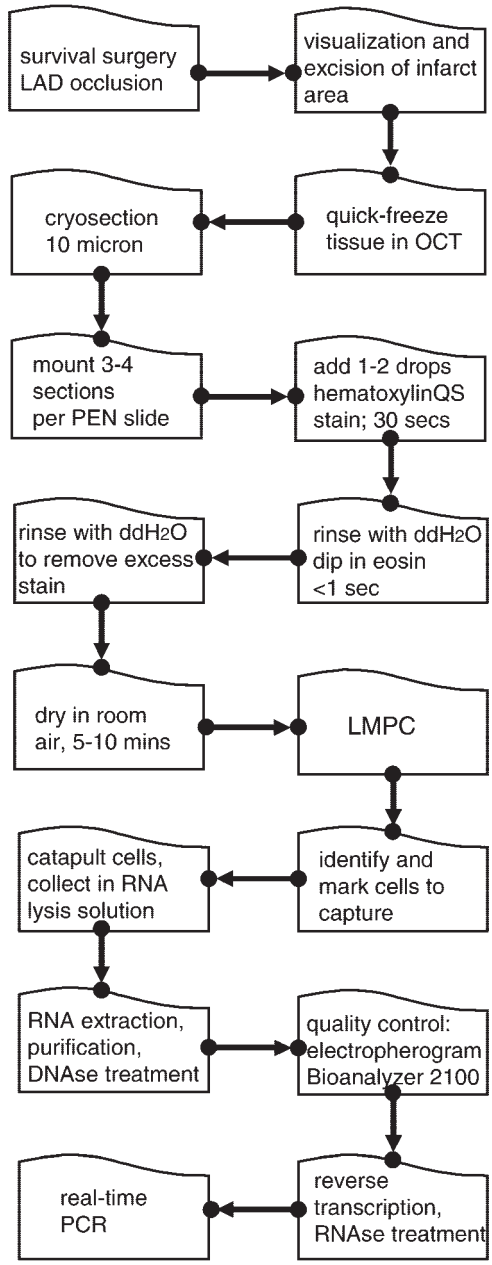

Fig. 9. Summarized protocol for the determination of gene expression from cell-specific LMPC tissue elements captured from the I, PI, or NI regions in a mouse heart section. Frozen blocks of tissue were sectioned, cDNA was prepared from histologically (tH&E) defined regions, and specific gene expression was analyzed in <1 working day. LAD, left anterior descending coronary artery; ddH_2O, double-distilled water; OCT, optimum cutting temperature; PEN, polyethylene napthalate.

blast differentiation by oxygen-sensitive signal transduction pathways (24–27). This "perceived hyperoxia" paradigm of myocardial remodeling has been recently reviewed (11, 30). Spatially resolved molecular analysis of infarcted myocardial tissue has been hindered by the lack of microdissection techniques to collect tissue samples with micron-level precision from infarct, peri-infarct, and noninfarct regions. Recently, we have addressed that need by developing a LMPC technique that is capable of dissecting infarct and peri-infarct regions of the heart. The tissue collected as such can be used for the study of gene expression in multicellular heart regions (20). However, the staining and microdissection procedures reported are not applicable to capture and analyze single cells. Postinfarction remodeling includes progressive loss of myocytes (1, 19) and a phenotypic switch of fibroblasts to myofibroblasts (24–27) in the peri-infarct region. It would be of extraordinary interest to understand the cell-specific biological mechanisms that cause such changes. At present, the cell-specific study of the intact myocardium is limited to histological approaches. The ability to capture myocardial tissue with a single cell resolution provides unprecedented power in performing quantitative genetic analyses on individual cell populations from specific regions of the heart. The technique reported herein accomplishes that goal.

p21 was originally described as functioning as a cell cycle regulator via inhibition of both cyclin-dependent kinases and DNA replication. More recently, it has been implicated in several fundamental processes, including transcriptional regulation and the modulation of apoptosis (8). p21 is mainly regulated at the transcriptional level (12). Previously, we had demonstrated that, in cardiac fibroblasts, inducible p21 expression is oxygen sensitive (24). That observation led to the paradigm of perceived hyperoxia which postulates that sublethal hyperoxic shock in the peri-infarct region of the ischemic heart results in differentiation of cardiac fibroblasts to myofibroblasts (25, 27, 30). In this study we obtained first evidence demonstrating that, in response to ischemia-reperfusion, the induction of p21 is not limited to cardiac fibroblasts but is also noted in cardiomyocytes. Whereas p21 function has been described as being important in cardiac development (15), the significance of p21 expression in peri-infarct myocytes remains unclear. Ischemia-reperfusion induces DNA damage (22). It is plausible that the induction of p21 in peri-infarct myocytes is aimed at DNA repair and survival (13). What factors override this protective response to trigger progressive myocytes loss in the postinfarcted myocardium remain to be identified.

Although standard immunohistological procedures are useful to identify specific cell types in the myocardial tissue, such an approach is not compatible with LMPC analyses because of the degradation of RNA during such staining.

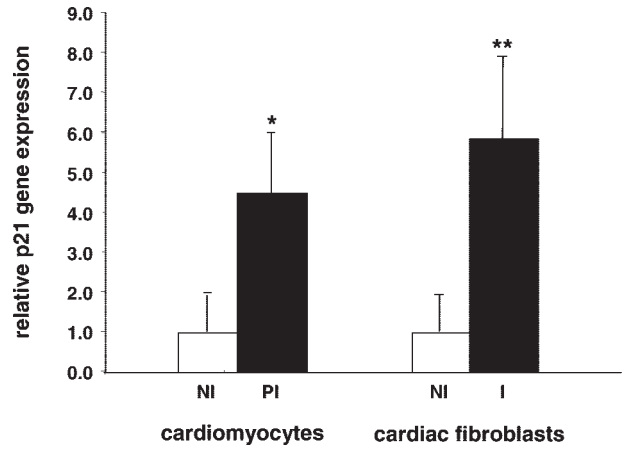

Fig. 10. Quantitative analysis of p21/Cip1/Waf1/Sdi1 gene expression using laser captured myocyte and fibroblast material. Cycle threshold values from real-time PCR were normalized to GAPDH expression. *$P < 0.005$, significantly different from PI region value; **$P < 0.001$, significantly different from infarct region value.

This work reports a novel LMPC-based technique to capture myocytes and fibroblasts from specific regions of the ischemia-reperfused myocardium. Cells captured with the use of this approach may be subjected to quantitative analyses of gene expression. To confirm the identity of the specific cell types being captured, it is important to subject the immediate serial section of the same tissue to immunohistochemical staining by using appropriate antibody against cell-specific antigens. Previously, we have presented histological evidence demonstrating that perceived hyperoxia induces p21 expression in the peri-infarct region of the ischemia-reperfused heart. Using the LMPC technique developed in this work, we report that p21 gene expression is significantly upregulated in the peri-infarct region of ischemia-reperfused heart. The induction is not limited to cardiac fibroblasts but is also noted in cardiomyocytes. Application of the novel LMPC technique developed in this study to understand spatially resolved cell-specific biological responses in the peri-infarct region of the reperfused heart should provide a new dimension in our understanding of myocardial healing.

ACKNOWLEDGMENTS

This study was supported by National Heart, Lung, and Blood Institute Grant RO1-HL-073087.

REFERENCES

1. **Abbate A, Biondi-Zoccai GG, Baldi A.** Pathophysiologic role of myocardial apoptosis in post-infarction left ventricular remodeling. *J Cell Physiol* 193: 145–153, 2002.
2. **Ai J, Tan Y, Ying W, Hong Y, Liu S, Wu M, Qian X, Wang H.** Proteome analysis of hepatocellular carcinoma by laser capture microdissection. *Proteomics* 6: 538–546, 2006.
3. **Bazan V, La Rocca G, Corsale S, Agnese V, Macaluso M, Migliavacca M, Gregorio V, Cascio S, Sisto PS, Di Fede G, Buscemi M, Fiorentino E, Passantino R, Morello V, Tomasino RM, Russo A.** Laser pressure catapulting (LPC): optimization LPC-system and genotyping of colorectal carcinomas. *J Cell Physiol* 202: 503–509, 2005.
4. **Bonner RF, Emmert-Buck M, Cole K, Pohida T, Chuaqui R, Goldstein S, Liotta LA.** Laser capture microdissection: molecular analysis of tissue. *Science* 278: 1481–1483, 1997.
5. **Burgemeister R.** New aspects of laser microdissection in research and routine. *J Histochem Cytochem* 53: 409–412, 2005.
6. **Chang MC, Chang YT, Tien YW, Sun CT, Wu MS, Lin JT.** Distinct chromosomal aberrations of ampulla of Vater and pancreatic head cancers detected by laser capture microdissection and comparative genomic hybridization. *Oncol Rep* 14: 867–872, 2005.
7. **Chew K, Rooney PH, Cruickshank ME, Murray GI.** Laser capture microdissection and PCR for analysis of human papilloma virus infection. *Methods Mol Biol* 293: 295–300, 2005.
8. **Child ES, Mann DJ.** The intricacies of p21 phosphorylation: protein/protein interactions, subcellular localization and stability. *Cell Cycle* 5: 1313–1319, 2006.
9. **Colantonio DA, Van Eyk JE, Przyklenk K.** Stunned peri-infarct canine myocardium is characterized by degradation of troponin T, not troponin I. *Cardiovasc Res* 63: 217–225, 2004.
10. **Emmert-Buck MR, Bonner RF, Smith PD, Chuaqui RF, Zhuang Z, Goldstein SR, Weiss RA, Liotta LA.** Laser capture microdissection. *Science* 274: 998–1001, 1996.
11. **Frangogiannis NF.** The mechanistic basis of infarct healing. *Antioxid Redox Signal* 8: 1907–1940, 2006.
12. **Gartel AL, Radhakrishnan SK.** Lost in transcription: p21 repression, mechanisms, and consequences. *Cancer Res* 65: 3980–3985, 2005.
13. **Golubnitschaja O, Moenkemann H, Trog DB, Blom HJ, De Vriese AS.** Activation of genes inducing cell-cycle arrest and of increased DNA repair in the hearts of rats with early streptozotocin-induced diabetes mellitus. *Med Sci Monit* 12: BR68–BR74, 2006.
14. **Guo J, Colgan TJ, DeSouza LV, Rodrigues MJ, Romaschin AD, Siu KW.** Direct analysis of laser capture microdissected endometrial carcinoma and epithelium by matrix-assisted laser desorption/ionization mass spectrometry. *Rapid Commun Mass Spectrom* 19: 2762–2766, 2005.
15. **Horky M, Kuchtickova S, Vojtesek B, Kolar F.** Induction of cell-cycle inhibitor p21 in rat ventricular myocytes during early postnatal transition from hyperplasia to hypertrophy. *Physiol Res* 46: 233–235, 1997.
16. **Hu Q, Wang X, Lee J, Mansoor A, Liu J, Zeng L, Swingen C, Zhang G, Feygin J, Ochiai K, Bransford TL, From AH, Bache RJ, Zhang J.** Profound bioenergetic abnormalities in peri-infarct myocardial regions. *Am J Physiol Heart Circ Physiol* 291: H648–H657, 2006.
17. **Jackson KA, Majka SM, Wang H, Pocius J, Hartley CJ, Majesky MW, Entman ML, Michael LH, Hirschi KK, Goodell MA.** Regeneration of ischemic cardiac muscle and vascular endothelium by adult stem cells. *J Clin Invest* 107: 1395–1402, 2001.
18. **Krause BJ, Poeppel TD, Reinhardt M, Vester EG, Yong M, Mau J, Strauer BE, Vosberg H, Muller HW.** Myocardial perfusion/metabolism mismatch and ventricular arrhythmias in the chronic post infarction state. *Nuklearmedizin* 44: 69–75, 2005.
19. **Krijnen PA, Nijmeijer R, Meijer CJ, Visser CA, Hack CE, Niessen HW.** Apoptosis in myocardial ischaemia and infarction. *J Clin Pathol* 55: 801–811, 2002.
20. **Kuhn DE, Roy S, Radtke J, Gupta S, Sen CK.** Laser microdissection and pressure-catapulting technique to study gene expression in the reoxygenated myocardium. *Am J Physiol Heart Circ Physiol* 290: H2625–H2632, 2006.
21. **Lawrie LC, Curran S.** Laser capture microdissection and colorectal cancer proteomics. *Methods Mol Biol* 293: 245–253, 2005.
22. **Lopez-Neblina F, Toledo AH, Toledo-Pereyra LH.** Molecular biology of apoptosis in ischemia and reperfusion. *J Invest Surg* 18: 335–350, 2005.
23. **Pijuan L, Vicioso L, Bellosillo B, Ferrer MD, Baro T, Pedro C, Lloreta-Trull J, Munne A, Serrano S.** CD20-negative T-cell-rich B-cell lymphoma as a progression of a nodular lymphocyte-predominant Hodgkin's lymphoma treated with rituximab: a molecular analysis using laser capture microdissection. *Am J Surg Pathol* 29: 1399–1403, 2005.
24. **Roy S, Khanna S, Bickerstaff AA, Subramanian SV, Atalay M, Bierl M, Pendyala S, Levy D, Sharma N, Venojarvi M, Strauch A, Orosz CG, Sen CK.** Oxygen sensing by primary cardiac fibroblasts: a key role of p21(Waf1/Cip1/Sdi1). *Circ Res* 92: 264–271, 2003.
25. **Roy S, Khanna S, Kuhn DE, Rink C, Williams WT, Zweier JL, Sen CK.** Transcriptome analysis of the ischemia-reperfused remodeling myocardium: temporal changes in inflammation and extracellular matrix. *Physiol Genomics* 25: 364–374, 2006.
26. **Roy S, Khanna S, Sen CK.** Perceived hyperoxia: oxygen-regulated signal transduction pathways in the heart. *Methods Enzymol* 381: 133–139, 2004.
27. **Roy S, Khanna S, Wallace WA, Lappalainen J, Rink C, Cardounel AJ, Zweier JL, Sen CK.** Characterization of perceived hyperoxia in isolated primary cardiac fibroblasts and in the reoxygenated heart. *J Biol Chem* 278: 47129–47135, 2003.
28. **Rumsey WL, Pawlowski M, Lejavardi N, Wilson DF.** Oxygen pressure distribution in the heart in vivo and evaluation of the ischemic "border zone". *Am J Physiol Heart Circ Physiol* 266: H1676–H1680, 1994.
29. **Scorsin M, Marotte F, Sabri A, Le Dref O, Demirag M, Samuel JL, Rappaport L, Menasche P.** Can grafted cardiomyocytes colonize peri-infarct myocardial areas? *Circulation* 94: II337–II340, 1996.
30. **Sen CK, Khanna S, Roy S.** Perceived hyperoxia: oxygen-induced remodeling of the reoxygenated heart. *Cardiovasc Res* 71: 280–288, 2006.
31. **Wang Y, Haider HK, Ahmad N, Xu M, Ge R, Ashraf M.** Combining pharmacological mobilization with intramyocardial delivery of bone marrow cells over-expressing VEGF is more effective for cardiac repair. *J Mol Cell Cardiol* 40: 736–745, 2006.
32. **Woo YJ, Panlilio CM, Cheng RK, Liao GP, Atluri P, Hsu VM, Cohen JE, Chaudhry HW.** Therapeutic delivery of cyclin A2 induces myocardial regeneration and enhances cardiac function in ischemic heart failure. *Circulation* 114: I206–I213, 2006.